Conference Paper

Kinematics of a Two Movable Disintegrator with Drives Based on the Bennett's Mechanism

M G Yarullin and F F Khabibullin

Department of Mechanical Engineering and Engineering Graphics, Kazan National Research Technical University named after A.N. Tupolev, Russia

Abstract

Important factor in the crushing and activation of building materials is the linear velocity of the working organs of the disintegrator. This paper consider the nature of the change of this parameter, as well as the linear velocity of the working element characteristic points. Their values are determined by three independent methods: analytical calculation, CAD / CAE analysis and experimental measurements. The results are compared and analyzed.

Corresponding Author:
M G Yarullin
Yarullinmg@yahoo.com
F F Khabibullin
fanil_arsk@mail.ru

Received: 10 February 2018
Accepted: 14 April 2018
Published: 7 May 2018

Publishing services provided by Knowledge E

Selection and Peer-review under the responsibility of the RFYS Conference Committee.

1. Introduction

Important factors of crushing and activation of building materials are the linear velocity of characteristic points and the angular velocity of the disintegrator working organs. As a result of crushing, activation of fine materials takes place, which is expressed in a number of cases by an increased ability to react in the course of subsequent technological operations. The activated state of the crushed material is characterized by its energy content, consisting of surface energy and crystal lattice distortion energy.

After researching many types of modifications of the Bennett's mechanism [1-6], we designed the design of a highly efficient new disintegrator. Its drives are developed on the basis of a parallelogram and antiparallelogram of the Bennett's mechanism (Figure 1) [7]. Drives provide high-quality and efficient grinding of the material due to uneven rotation of the working members [8-12].

To ensure the uneven rotation of the working cones of the disintegrator, a parallelogram and antiparallelogram Bennett was used in its drive.

Dependency between kinematic parameters of the Bennett mechanism crankshafts and the movement law (angle of rotation) of the leading crank looks like:

$$\gamma = \arcsin\left(\frac{-\cos\alpha_3 \cdot \sin\phi}{1-\sin\alpha_3 \cdot \cos\phi}\right), \gamma = \arccos\left(\frac{\cos\phi - \sin\alpha_3}{1-\sin\alpha_3 \cdot \cos\phi}\right) \quad (1)$$

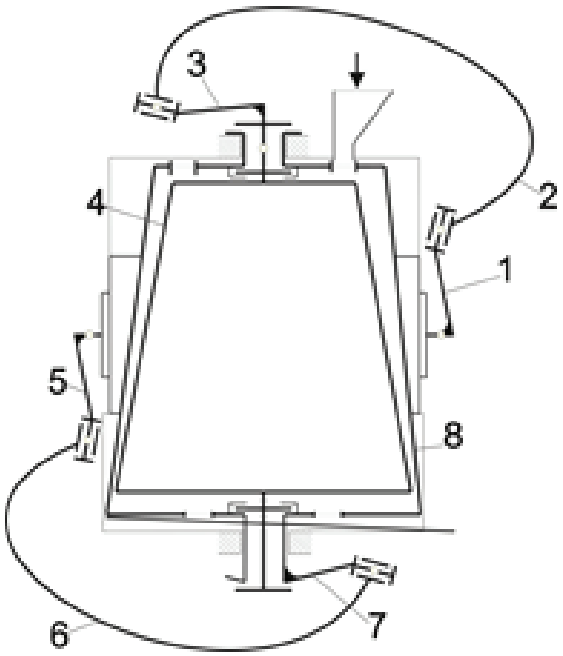

Figure 1: Structural diagram of the disintegrator.

Angle γ is not proportional to the angle ϕ. Differentiating one of the expressions (1) with respect to time, we obtain the angular velocity [13]:

$$\omega_3 = -\omega_1 \cdot \cos\alpha_1/(1 - \sin\alpha_1 \cdot \cos\phi) \tag{2}$$

Expression (2) shows that at ω_1= const the angular velocity of the crankω_3 is not a constant, but depends on the leading crank crossing angle $\alpha_1$and on the angle ϕ of its turn.

Moreover, for a fixed value α_1, the angular velocity of the driven crank ω_3 reaches its maximum value in absolute value at ϕ= 0, and the minimum atϕ = 180 °:

$$\omega_{3\,\max} = \omega_1 \cdot \cos\alpha_1/(1 - \sin\alpha_1), \tag{3}$$

$$\omega_{3\,\min} = \omega_1 \cdot \cos\alpha_1/(1 + \sin\alpha_1) \tag{4}$$

Inequality of rotation of the driven crank [14, 15]:

$$\delta = \pm 2\frac{\sin\alpha_1 \cdot \sin\alpha_2}{\cos\alpha_2 - \cos\alpha_1}.$$

A graphic interpretation of this equation is given in the Figure 2.

When designing the disintegrator drive in order to simplify the technology of manufacturing the drive links, the angle α_2 should preferably be taken equal to 90 degrees. For this case, the formula for calculating the non-uniformity coefficient [16] has the form

$$\delta = 2 \cdot tg\alpha_1 \tag{5}$$

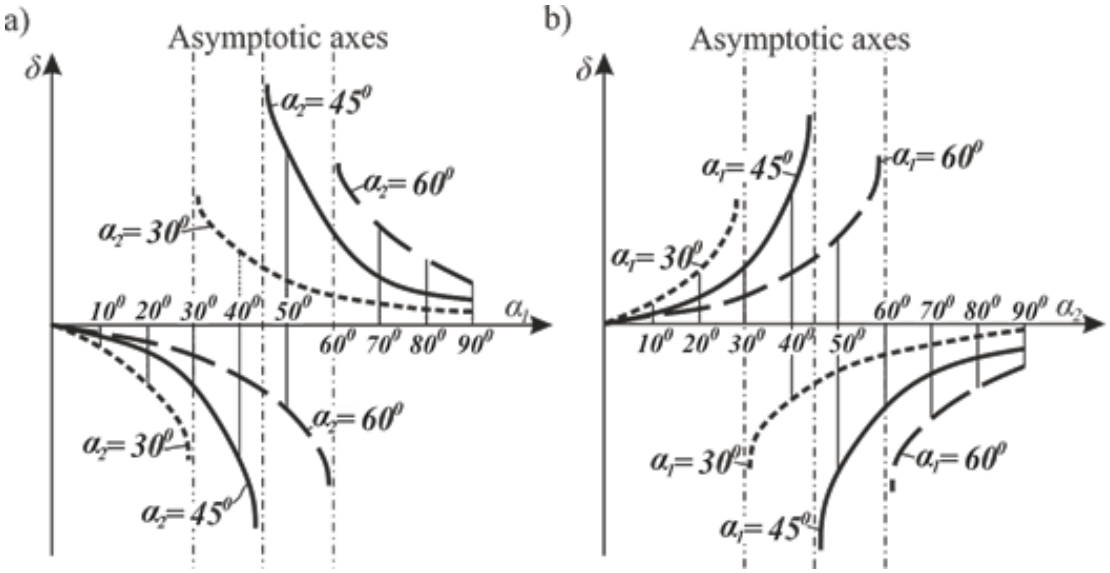

Figure 2: Graphs of variation in the uneven rotation of the crank of the Bennett mechanism a) $\delta = f(\alpha_1)$ at $\alpha_1 = 30^0, 45^0$and 60^0b)$\delta = f(\alpha_2)$ at $\alpha_2 = 30^0, 45^0$and 60^0.

or

$$\delta = 2 \cdot tg\alpha_1 = (\omega_{3\,\max} - \omega_{3\,\min})/\omega_{3ave} \tag{6}$$

Here it is assumed that $\omega_{3\,ave} = \omega_{1.}$

To differentiate the expression (4) with respect to time, we obtain the angular acceleration of the driven crank:

$$\epsilon_3 = \omega_1^2 \cdot \sin\alpha_1 \cdot \cos\alpha_1 \cdot \sin\phi/(1 - \sin\alpha_1 \cdot \cos\phi)^2 \tag{7}$$

Analysis of the obtained equations (2) - (6) shows that the motion of the driven crank is non-uniform (Figure 3). This in turn leads to uneven movement of the disintegrator's working organs, as a result of which the processes of dispersion and activation will take place in a medium with varying angular velocities, angular accelerations, i.e. more intensively.

A change in the radius of the working bodies leads to a change in the value of the angular velocity and acceleration in the working chamber.

2. Linear speed of the working element

To study the kinematic parameters of the driven cranks (working disintegrator cones) along with the mathematical model of the disintegrator kinematics (expressions 3-7), its 3D model was developed and experimental measurements were made. Studies of the results of kinematics by the above listed independent three methods have made it possible to verify the correctness of the models obtained.

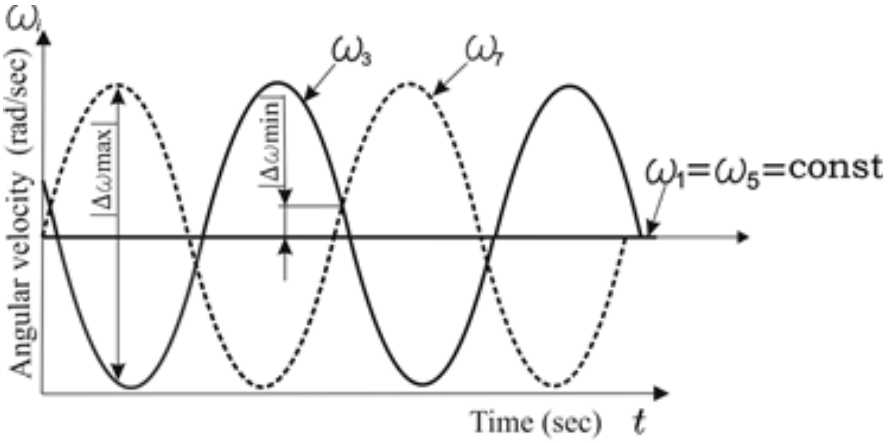

Figure 3: The graph of the angular velocities of the leading (1, 5) and slave (3, 7) cranks.

We introduce the notion of "characteristic points" located on the generatrix of the cone line through fixed distances (Figure 4). For the convenience of technical measurements, characteristic points are taken in accordance with Figure 4: l_1=15 mm, l_2=90 mm, l_3=115 mm and correspondingly, r_1=60 mm, r_2=57.19 mm, r_3=45.9 mm, as well as the frequency of rotation of the driven link, we take n=120 min^{-1}. Angular velocity accepted ω=12.56 sec^{-1}.

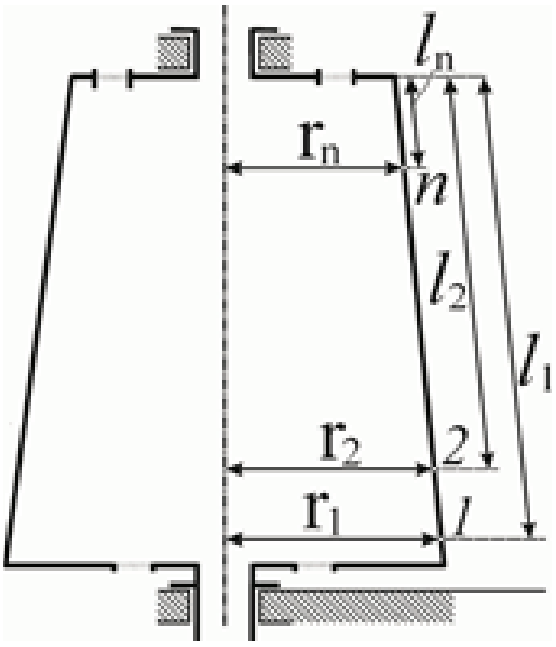

Figure 4: Coordinates of the location of characteristic points on the working cone.

2.1. Method of analytical calculations

The value of the average linear velocity at the selected characteristic points is determined by the formula (8):

$$V_{n-mid}^{th} = \omega \cdot r_n \tag{8}$$

where ω- angular velocity of the cone, rad/sec;

r_n- radius of a cone at a characteristic point, mm.

The results of analytical calculations of the average linear velocity are given in table 1.

Table 1: The values of linear velocities obtained by CAD / CAE analysis.

r_n, mm	60	57	46
V_{n-mid}^{th}, mm/sec	753.6	717.1	576.5

2.2. Method of CAD / CAE analysis

CAD / CAE analysis of the 3D model of the disintegrator allows to obtain graphs of linear velocity changes at characteristic points (Figure 5).

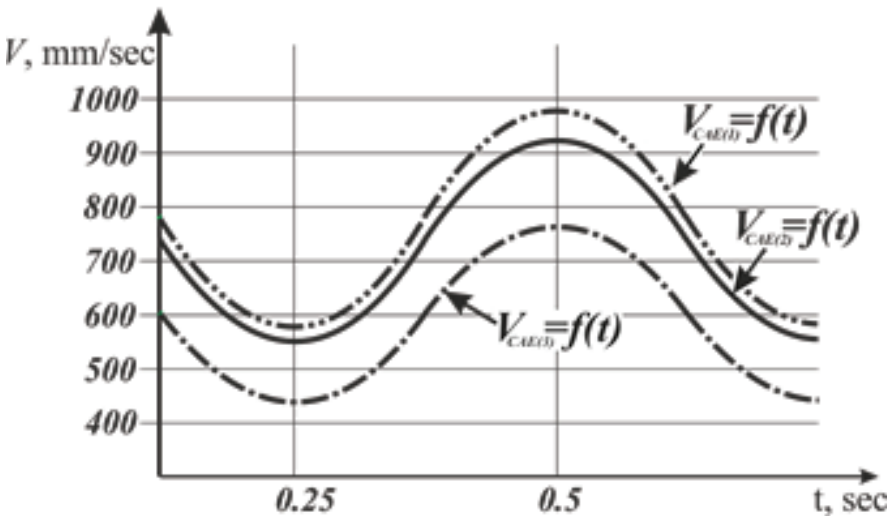

Figure 5: Graph of changes in linear velocities at characteristic points.

Analysis of the graph of changes in linear velocities shows that the driven crank rotates at a variable speed. The maximum linear velocity of the characteristic point at

a radius of r = 60 mm is 984 mm/sec, the minimum linear velocity is 580 mm/sec. The average value of the linear velocity is determined by formula (9)

$$V_{1-mid}^{CAE} = \frac{V_{1-\max}^{CAE} + V_{1-\min}^{CAE}}{2} \quad (9)$$

In a similar way, the linear velocity parameters are determined (table 2).

Table 2: The values of linear velocities obtained by CAD / CAE analysis.

l_n, mm	r_n, mm	V_n^{CAE}, mm/sec		V_{n-mid}^{CAE}, mm/sec
		max	min	
115	60	984	580	782
90	57.19	936	556	746
15	45.9	750	446	598

2.3. Method of experimental measurements

Measurements of the linear velocity of the surface of the outer cone were made for the same characteristic points by the digital tachometer ATT-6001. The maximum $V_{n-\max}^{\exp}$, minimum $V_{n-\min}^{\exp}$, and average linear velocities $V_{n-mid}^{\exp}$ were measured.

In order to obtain a more accurate average total value, the maximum and minimum parameters of the linear velocity at each characteristic point, the measurements were carried out by fivefold repetition. The obtained parameters are presented in table 3.

Table 3: The values of the linear velocities are.

l_n, mm	$V_n^{\exp}$, mm/sec		$V_{n-mid}^{\exp}$, mm/sec
	max	min	
115	833.666	749.566	791.616
90	806.333	724.333	765.333
15	659.833	601.866	630.849

3. Data analysis

To analyze and compare the results of the investigated linear velocities obtained above by the three independed methods, table 4 and figures 6,7 are given.

Table 4: The values of the linear velocities obtained by analytical, CAD / CAE and experimental methods.

Coordinates of characteristic points l_n, mm	Values of linear velocities, mm/sec						
	Analytical method	Method CAD/CAE analysis			The experimental method		
		max	min	mid	max	min	mid
115	753.6	984	580	782	833.666	749.566	791.616
90	717.1	936	556	746	806.333	724.333	765.333
15	576.5	750	446	598	659.833	601.866	630.849

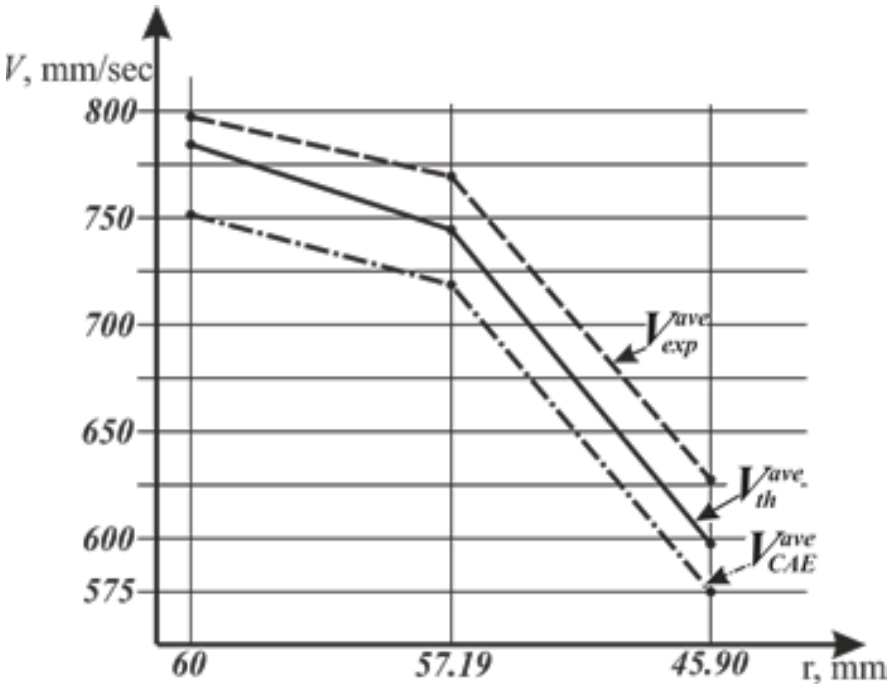

Figure 6: Graph of changes of average linear velocity.

The graph of the changes of average linear velocity along the vertical axis shows the parameters of the linear velocity (mm/sec), along the horizontal axis the parameters of the radius of the outer cone (mm) are presented. The difference between the average values of the characteristic points of theoretical, computer and experimental data will confirm the degree of adequacy of the results obtained.

The maximum and minimum parameters (extremes) of the linear velocity of the non-uniform rotation of the computer model must coincide with the corresponding maximum and minimum parameters obtained experimentally.

$$\Delta\omega_{n-\max} = \omega_{n-\max}^{CAE} - \omega_{n-\max}^{\exp} \Rightarrow 0$$

$$\Delta\omega_{n-\min} = \omega_{n-\min}^{CAE} - \omega_{n-\min}^{\exp} \Rightarrow 0$$

Based on the parameters obtained at r_1 = 60 mm, a graph of extremum points is given, shown in Figure 7.

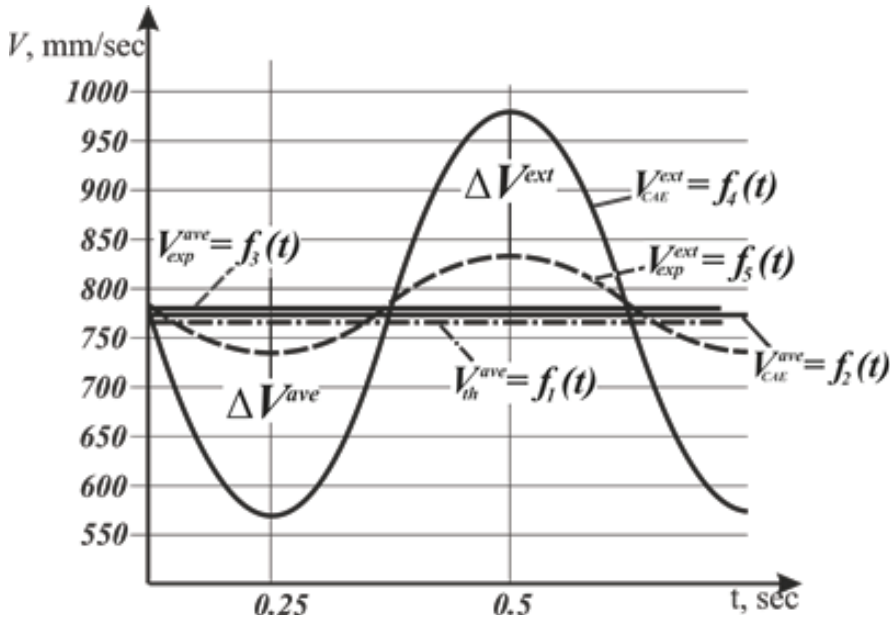

Figure 7: Graphs of extreme and average values of linear velocity at r_1 = 60 mm.

4. Conclusion

Analysis of the velocity graphs presented in Figure 7 shows that the maximum difference between the average velocities is 38 mm/sec, which is no more than 4.92% of the relative error. The difference between the extremum values (maximum, minimum) is 16.53% relative error. That is explained by the fact that the CAD / CAE method does not take into account the moments of inertia of the cones and the effect of the unequal rotation of the driven link on the leading link.

Reducing the unevenness of the cone rotation for a real installation for the above reasons has a positive effect on the dynamics of the disintegrator, nevertheless, the unevenness of the cone rotation positively influences the dynamics of the process of material destruction. Thus, the results of a study of the kinematics of the disintegrator cone characteristic points are: firstly, the initial material for investigating the

dynamics of crushing, determining the optimum operating mode and the performance of the device; Secondly, it confirms the correctness of the theoretical, computer and experimental studies obtained.

References

[1] Bennett G T 1903 A new mechanism *Engineering* p.777-778.

[2] Alizade R I, Kiper G and Bagdadioglu B 2014 Function synthesis of Bennett 6R mechanisms using Chebyshev approximation *Mech Mach Theory* **81** p. 62–78.

[3] McCarthy J 2000 Geometric Design of Linkages *Springer* 320 p.

[4] Budniak Z and Bil T 2012 Simulation of the movement of four-bar spatial linkage *Int. J. of Applied Mechanics and Engineering* **Vol. 17** p.723-732.

[5] Lee C C and Herve J M 2014 Oblique circular torus, Villarceau circles, and four types of Bennett linkages *Part C J Mech Eng Sci*. **228(4)** p. 742-752.

[6] Lee C C and Herve J M 2015 The Metamorphic Bennett Linkages *The 14th IFToMM World Congress,* Taipei, Taiwan.

[7] Pat. **2581487** 2016 Russian Federation, Disintegrator of uneven crushing Yarullin M G, Mingazov M R, Isyanov I R and Khabibullin F F publ. 04/20/2016 Byul. № 11-9 p.

[8] Evgrafov A N 2013 Calculation of geometric and kinematic parameters of the spatial lever mechanism with redundant coupling *Problems of machine building and machine reliability* **No.3** p. 3-8.

[9] Herve J M 2009 Conjugation in the displacement group and mobility in mechanisms *Transactions of the Canadian Society for Mechanical Engineering* **Vol. 33** p. 163–174.

[10] Yarullin M G, Mingazov M R and Galiullin I A 2016 Historical review of studies of spatial nR linkages *International Review of Mechanical Engineering* **10(5)** p. 348-356.

[11] Herve J M and Dahan M 1983 The two kinds of Bennett's mechanisms S*ixth IFToMM World Congress on Theory of Machines and Mechanisms* **Vol.1** p. 116-119.

[12] Lee C C and Herve J M 2010 Generators of the product of two Schoenflies motion groups *Euro. J. Mech A/Solids* **29(1)**p. 97–108.

[13] Yarullin M G, Khabibullin F F and Isyanov I R 2016 Nonlinear crushing dynamics in two degree of freedom disintegrator based on the Bennett's linkage *Vibroengineering procedia* **Vol. 8** p. 477- 482.

[14] Yarullin M G and Mingazov M R 2016 Structural modifications synthesis of Bennett mechanism *Lecture Notes in Mechanical Engineering* p. 9-16.

[15] Yarullin M G and Khabibullin F F 2017 Theoretical and Practical Conditions of Bennett Mechanism Workability *Lecture Notes in Mechanical Engineering* p. 145-153.

[16] Mudrov P G 1976 Spatial mechanisms with rotational pairs *Publishing House of Kazan University*p. 264.